Upscaling Tensorial Permeability Fields Based on Gaussian Markov Random Field Models and the Hybrid Mixed Finite Element Method

Zhuoxin Bi, SPE, J. Trangenstein, D. Higdon, H. Lee, Duke University

This paper was prepared for presentation at the 2002 SPE Annual Technical Conference and Exhibition held in San Antonio, Texas, 29 September - 02 October 2002.

Abstract

In this paper, a fine scale simulation-based upscaling procedure for full tensor permeability fields is presented based on the Hybrid Mixed Finite Element (HMFE) numerical scheme and synthetic permeability fields generated using a Gaussian Markov Random Field (GMRF) model. HMFE scheme is an accurate scheme that conveniently represents tensorial permeability field for forward flow/transport simulation. It is also one of few choices that provides a natural technique for conservative upscaling, meaning that the coarse grid should produce the same flux and pressure as the upscaled fine values. As in any renormalization approach, we require that the coarse linear system to be in the same form as in the fine. This process produces good upscaling results if both the fine scale tensor and the upscaled tensor are assumed diagonal. However, results from a few examples show that it is not always possible to obtain a positive definite permeability tensor while conserving fluxes and pressures on upscaled cells. One explanation is that the discretized Darcy's law on the upscaled grid, based on conserving fine flow variables, may not be valid. Results from a generally used two-step upscaling procedure demonstrate that a symmetric, positive definite tensor field on coarser grids is obtainable. But it should be applied with caution because some of the off-diagonal values may be highly unreasonable.

Introduction

Upscaling of permeability heterogeneity can be thought of as a spatial resolution transformation from a geological model built on a very fine grid to a numerical permeability model on a full-field flow simulation grid. A great deal of research work has been done in the last few decades and different upscaling approaches have been proposed and applied in practice, from the simple averaging (arithmetic, harmonic and geometric) to the more complicated renormalization [16], homogenization [8,13,14] and the simulation-based approaches [4,7,10,15]. Common upscaling approaches such as renormalization, homogenization, etc. are based on 1D ideas and the tensor extensions are 1D after a rotation. Different approaches rely on different upscaling criteria such as conservation of statistics [6,9,18], conservation of mean flow [10,12,13], or energy dissipation [9], and even preservation of the governing PDEs [8,13].

There is a good agreement that upscaling results are problem dependent, that is, the upscaling results depend not only on the intrinsic permeability heterogeneity but also on the boundary conditions of the flow problem [2,3]. To distinguish these problem dependent consequences from the intrinsic properties of the porous media, a few concepts or definitions have been adopted both in the reservoir engineering community and the underground hydrology community. Block or efficient permeability is usually referred to the upscaling results.

The importance of full tensorial representation of porous media permeability has been reported by many researchers [3]. Upscaling of a tensor permeability field relies not only on a tensorial representation scheme but also on an effective approach.

In this paper, we are trying neither to review and compare different approaches nor to propose another completely new method. Rather, we adapt the simulation-based upscaling strategy as reported by many investigators, but concentrate on a relatively new numerical simulation method, i.e., the Hybrid Mixed Finite Element method(HMFE) and a Gaussian Markov Random Field (GMRF) model for permeability. MRF models have been used before as permeability models[20]. Our HMFE schemes

emplying adaptive mesh refinement techniques are useful for flow and transport simulation in porous media. Upscaling is only a basic by-product. A short description of this method and its advantages are given in the next section.

Gaussian Markov random field models have been widely and successfully used in image analysis for a long time[19,21,22]. It is essentially a Gaussian random field model for which spatial dependence is specified through local interactions. Such models can offer advantages both in modeling and computation as compared to standard geostatistical models.

The main idea of the simulation-based upscaling approaches is to conserve the fine flow field (flux and pressure) obtained from a relatively simple and cheaper simulation on the discrete fine domain by an efficient or smoother version of the fine scale heterogeneity (permeability).

Following many authors [4,5,7,11,12,13,17], we consider single phase incompressible flow in a 2D isothermal porous medium, e.g., an oil reservoir or a underground aquifer. We denote the flow region and its boundary as Ω and $\partial\Omega$, respectively. The concerning flow variables for upscaling purposes are fluid pressure $P(x,y)$ and volumetric flux $\mathbf{V}(x,y)$, which are functions of space coordinates $(x,y) \in \Omega$. We assume that the local-scale Darcy's law and the continuum approach apply. In this approach, the continuous porous medium is replaced by a fictitious continuum where we can represent the medium with physically meaningful parameters on a representative elementary volume (REV) such as porosity $\phi(x,y)$ and permeability $K(x,y)$ and take the flow variables as continuous functions of space (and time in general). The local Darcy's law provides a relationship between the volumetric flux and the pressure gradient. Under an incompressible medium assumption, the local-scale governing equations based on mass conservation and Darcy's law can be written as,

$$\mathbf{V}(x,y) = -\frac{K(x,y)}{\mu}\nabla P(x,y), \tag{1}$$

$$\nabla \cdot \mathbf{V}(x,y) = 0, \tag{2}$$

where μ is the fluid viscosity which will be considered constant.

To simplify notation, we will denote $P(x,y) = P$, $\mathbf{V}(x,y) = \mathbf{V}$ and $T(x,y) = \frac{K(x,y)}{\mu}$, called transmissibility, from now on and assume $\mu = 1cp$, without loss of generality, so that $T(x,y)$ is equivalent to $K(x,y)$ in value. It should be noted that the medium heterogeneity is represented in the equation by $K(x,y)$. $K(x,y)$ or $T(x,y)$ is a positive definite tensor field in nature. This parameter, appearing as functions of spatial coordinates (x,y), is termed as a spatial field and its point-wise values have to be given to solve equations (1) and (2) for P and $\mathbf{V}$. In the last few decades, a great deal of research has been carried out on modeling $K(x,y)$ and the most widely used models are to treat $K(x,y)$ as a random spatial function or a random field. As a consequence, the flow variables, P and $\mathbf{V}$, are also random in nature. As stated previously, we will use GMRF models for $K(x,y)$.

In this paper, we seek to solve the equations (1) and (2) on a finite numerical domain of Ω that corresponds to a geological modeling grid by the HMFE method. We will denote this grid as $\tilde{\Omega} = \cup_{i=1}^{n_x} \cup_{j=1}^{n_y} \Omega_{ij}$ where n_x and n_y are the number of gridblocks in each coordinate direction of the geological domain $\tilde{\Omega}$. The upscaling problem of the random field $K(x,y)$ based on the simulation results on the domain $\tilde{\Omega}$ is defined as follows: (for simplicity, we drop the functional dependence of K on (x,y)) Given a realization of the GMRF permeability model on a geological grid $\tilde{\Omega}$, denoted by $\mathbf{k}$, and the numerical solution of Eqs. (1) and (2) by the HMFE scheme on this grid, find an upscaled version of $\mathbf{k}$, defined on $\tilde{\Omega}^c$ and denoted by $\mathbf{k}^c$, such that the volumetric fluxes and the driving pressures are the same on both scales.

It is important to be aware that there are a few assumptions made for this simulation-based upscaling process. Most importantly, for closure in renormalization, we assume that the discrete Darcy's law and divergence free equation of Eqs. (1) and (2) based on the HMFE discretization scheme are valid on the upscaled grid $\tilde{\Omega}^c$. Secondly, we assume that an upscaled, physically meaningful permeability tensor field can be obtained for each realization of K on a fine grid. We will see from the examples that these assumptions are not always simultaneously possible.

The Hybrid Mixed Finite Element Method

In the conventional approach employed in reservoir engineering, one combines Eqs. (1) and (2) and solves the pressure equation by finite difference or finite element methods, and the volumetric flux field is then determined by Darcy's law and numerical differentiation of the pressure solution. In this case, the flux field is one order less accurate than the pressure field. In addition, it does not produce flux and pressure at cell sides to allow formulation of a consistent upscaled block-centered models. In the HMFE method, however, we treat and discretize Eq.(1) and Eq.(2) separately, then solve directly for both the pressure and the flux field, that is, the so-called mixed formulation. This discretization conserves volume naturally. Under reasonable circumstances, it is known that the HMFE produces the same cell-centered pressures and volume fluxes as the lowest-order mixed method, which itself is related to block-centered finite differences. Another advantage of this formulation is that the full tensorial permeability field is represented very conveniently and the hybrid formulation of the mixed finite element method leads to a block diagonal linear system for side pressures. Although this system is larger than that for the mixed method, it is positive defi-

nite (unlike that of the mixed method).

Rather than giving a detailed formulation and discretization of the HMFE method, we refer interested readers to the paper by Trangenstein, etc.[1] for details and the Adaptive Mesh Refinement schemes. Instead, we provide the discretized equation on each rectangular element (or cell) of the geological grid $\tilde{\Omega}$. Using piece-wise constant pressure functions, discontinuous (linear,constant) or (constant,linear) velocities, piece-wise constant Lagrange multipliers, piece-wise constant permeabilities, and exact integration, within each cell Ω_{ij} on the geological grid $\tilde{\Omega}$, we can write Darcy's law (1) and the divergence-free equation (2) in the matrix form

$$\begin{bmatrix} \frac{1}{3}\frac{\triangle x}{\triangle y}k_{11}^{-1} & \frac{1}{6}\frac{\triangle x}{\triangle y}k_{11}^{-1} & \frac{1}{4}k_{12}^{-1} & \frac{1}{4}k_{12}^{-1} & 1 \\ \frac{1}{6}\frac{\triangle x}{\triangle y}k_{11}^{-1} & \frac{1}{3}\frac{\triangle x}{\triangle y}k_{11}^{-1} & \frac{1}{4}k_{12}^{-1} & \frac{1}{4}k_{12}^{-1} & -1 \\ \frac{1}{4}k_{21}^{-1} & \frac{1}{4}k_{21}^{-1} & \frac{1}{3}\frac{\triangle y}{\triangle x}k_{22}^{-1} & \frac{1}{6}\frac{\triangle y}{\triangle x}k_{22}^{-1} & 1 \\ \frac{1}{4}k_{21}^{-1} & \frac{1}{4}k_{21}^{-1} & \frac{1}{6}\frac{\triangle y}{\triangle x}k_{22}^{-1} & \frac{1}{3}\frac{\triangle y}{\triangle x}k_{22}^{-1} & -1 \\ 1 & -1 & 1 & -1 & 0 \end{bmatrix} \begin{bmatrix} V_{1L}\triangle y \\ V_{1R}\triangle y \\ V_{2L}\triangle x \\ V_{2R}\triangle x \\ P \end{bmatrix}$$

$$= \begin{bmatrix} P_{1L} \\ -P_{1R} \\ P_{2L} \\ -P_{2R} \\ -q \end{bmatrix}, \qquad (3)$$

where k_{11}^{-1}, k_{12}^{-1}, k_{21}^{-1} and k_{22}^{-1} denote the elements of the inverse of the permeability tensor (not the reciprocal of the tensor elements); P is the cell center pressure; q represents the production from the cell or injection into the cell. The cell sizes in the x- and y- coordinate directions are $\triangle x$ and $\triangle y$. Other notations are illustrated in Fig. 1, where the side pressures and velocities are considered to be at the centers of the sides and L and R means from the left and right of the sides. The linear system for side pressures, P_{1L}, P_{1R}, P_{2L} and P_{2R}, follows by inverting and using continuity of volume flux.

Upscaling Methodology

Given a realization of the random permeability model (either scalar or tensor) on the geological scale grid $\tilde{\Omega}$, we can solve Eq.(3) numerically for V_{1L}, V_{1R}, V_{2L} and V_{2R} as well as P_{1L}, P_{1R}, P_{2L} and P_{2R}. With this flow information, one can back solve the system of equations for the permeability tensor field on a coarser scale grid $\tilde{\Omega}_c$ by completely or partially conserving the flow properties such as fluid fluxes and driving fluid pressures.

The general upscaling procedures are as follows: we first generate a realization from the permeability model. Then we take the realization as the true permeability field on the fine-scale grid and use our AMR code with maximum level of refinement 1 (for uniform grid simulation) to do simulation for side pressures, side velocities and cell pressures (our AMR code libraries are designed for flow and transport simulation in porous media using Adaptive Mesh Refinement technologies, the cell size or scale of the numerical grid is modified dynamically during simulation. But it can be used for simulations on uniform grid with fixed scale or cell size). We then upscale these flow variables using conservation of flow variables with an upscaling factor of R (meaning R×R fine cells upscaled to one coarse cell) to get the flow variables on the coarse grid. Finally, we apply these upscaled flow variables to back solve the permeability field on the coarse grid as described in the following subsections.

Diagonal Tensor One way to solve Eq. (3) for permeability is to force the upscaled permeability tensor to be diagonal, i.e., $k_{12}^c = k_{21}^c = 0$. By doing this, we actually decouple the full tensorial system of equations into two separate scalar equations. Of course, the upscaling would be very simple. It is easy to see that the diagonal entries of the upscaled permeability are

$$k_{11}^c = \frac{\frac{1}{2}\triangle x(V_{1L}^c + V_{1R}^c)}{(P_{1L}^c - P_{1R}^c)}, \quad k_{22}^c = \frac{\frac{1}{2}\triangle y(V_{2L}^c + V_{2R}^c)}{(P_{2L}^c - P_{2R}^c)}. \qquad (4)$$

By default, all the variables in this equation are defined on a coarse cell overlapped on the corresponding fine cells. Given the fine cell values for V_{1L}, V_{1R}, V_{2L}, V_{2R} and P_{1L}, P_{1R}, P_{2L}, P_{2R}, one can actually calculate the corresponding coarse cell values by the definition of the physical properties (conservation of forces and fluxes). For example, conservation of fluid flux and pressure in the x-coordinate direction on the coarse grid gives

$$V_{1L}^c = \frac{\sum V_{1L}^f \triangle y^f}{\sum \triangle y^f}, \qquad P_{1R}^c = \frac{\sum P_{1R}^f \triangle y^f}{\sum \triangle y^f}, \qquad (5)$$

where the notations are obvious as shown in Fig. 2. Note that this is actually a linear transformation, hence the divergence equation (last equation in Eq.(3)) will be automatically satisfied on the coarse cell. Also note that the fine cell center pressure does not matter in this case.

It is not difficult to see that two steps are required in order to determine both k_{11}^c and k_{22}^c. During the step for k_{11}^c, fine scale flow caused by fine heterogeneity in the y-coordinate direction will be neglected. Similarly, fine scale flow in the x-direction will be neglected in the computation of k_{22}^c.

Symmetric Tensor Another way to determine the upscaled permeability tensor based on the fine flow variables is to assume a symmetric permeability tensor. In this case, the coarse cell center pressure could also be taken as an unknown because it is not clear how one should calculate it rather than to make it satisfy the HMFE discretization (Eq.(3)) on the coarse cell. Note that since there are four

equations and four unknowns, one can seek a unique solution as long as the coefficient matrix associated with the upscaled flow variables is not singular.

To show the process, we take k_{11}^{-1}, $k_{12}^{-1}=k_{21}^{-1}$, k_{22}^{-1} and P of a coarse cell composed of $R\times R$ fine cells as unknowns, use Eq.(5) for fluxes and side pressures and rewrite the matrix equation, Eq.(3), on the coarse cell, as follows,

$$\begin{bmatrix} \left(\frac{V_{1L}}{3}+\frac{V_{1R}}{6}\right)\triangle x & \frac{\triangle x}{4}\left(V_{2L}+V_{2R}\right) & 0 & 1 \\ \left(\frac{V_{1L}}{6}+\frac{V_{1R}}{3}\right)\triangle x & \frac{\triangle x}{4}\left(V_{2L}+V_{2R}\right) & 0 & -1 \\ 0 & \frac{\triangle y}{4}\left(V_{1L}+V_{1R}\right) & \left(\frac{V_{2L}}{3}+\frac{V_{2R}}{6}\right)\triangle y & 1 \\ 0 & \frac{\triangle y}{4}\left(V_{1L}+V_{1R}\right) & \left(\frac{V_{2L}}{6}+\frac{V_{2R}}{3}\right)\triangle y & -1 \end{bmatrix}$$

$$\times \begin{bmatrix} k_{11}^{-1} \\ k_{12}^{-1} \\ k_{22}^{-1} \\ P \end{bmatrix} = \begin{bmatrix} P_{1L} \\ -P_{1R} \\ P_{2L} \\ -P_{2R} \end{bmatrix}. \qquad (6)$$

Note that we have dropped the coarse cell indicator for simplicity. The solution of this matrix equation, if it exists, can be written as,

$$\begin{bmatrix} k_{11}^{-1} \\ k_{12}^{-1} \\ k_{22}^{-1} \\ P \end{bmatrix} = B \times \begin{bmatrix} P_{1L} \\ -P_{1R} \\ P_{2L} \\ -P_{2R} \end{bmatrix}, \qquad (7)$$

where B is the inverse of the coefficient matrix in Eq.(6). Note that k_{11}^{-1}, k_{12}^{-1} and k_{22}^{-1} are the entries of the inverse of the permeability tensor in the upscaled cell. It is easy to compute k_{11}, k_{12} and k_{22} from the entries of the inverse tensor,

$$k_{11}=\frac{k_{22}^{-1}}{k_{11}^{-1}k_{22}^{-1}-k_{12}^{-1}k_{12}^{-1}},\quad k_{22}=\frac{k_{11}^{-1}}{k_{11}^{-1}k_{22}^{-1}-k_{12}^{-1}k_{12}^{-1}},$$

and

$$k_{12}=k_{21}=-\frac{k_{12}^{-1}}{k_{11}^{-1}k_{22}^{-1}-k_{12}^{-1}k_{12}^{-1}}. \qquad (8)$$

It should be pointed out that there is no guarantee that the resulting symmetric permeability tensor is positive definite unless all the underlying upscaling assumptions are satisfied such that $k_{11}^{-1}>0, k_{22}^{-1}>0, k_{11}^{-1}k_{22}^{-1}-k_{12}^{-1}k_{12}^{-1}>0$.

Overdetermined Symmetric Tensor Case Finally, one can obtain a symmetric permeability tensor if the coarse cell center pressure P can be computed independently, say by volume averaging over the fine cell center pressures, i.e.,

$$P^c=\frac{\sum P^f\triangle x^f\triangle y^f}{\sum\triangle x^f\triangle y^f}. \qquad (9)$$

Since the solution in this case is over-determined (3 unknowns and 4 equations) , the singular value decomposition will be used for the solutions. The singular value decomposition produces a solution that is the best approximation in the least-square sense. Again, taking k_{11}^{-1}, $k_{12}^{-1}=k_{21}^{-1}$ and k_{22}^{-1} as unknowns and rearranging Eq.(3) result in

$$\begin{bmatrix} \left(\frac{V_{1L}}{3}+\frac{V_{1R}}{6}\right)\triangle x & \left(\frac{V_{2L}}{4}+\frac{V_{2R}}{4}\right)\triangle x & 0 \\ \left(\frac{V_{1L}}{6}+\frac{V_{1R}}{3}\right)\triangle x & \left(\frac{V_{2L}}{4}+\frac{V_{2R}}{4}\right)\triangle x & 0 \\ 0 & \left(\frac{V_{1L}}{4}+\frac{V_{1R}}{4}\right)\triangle y & \left(\frac{V_{2L}}{3}+\frac{V_{2R}}{6}\right)\triangle y \\ 0 & \left(\frac{V_{1L}}{4}+\frac{V_{1R}}{4}\right)\triangle y & \left(\frac{V_{2L}}{6}+\frac{V_{2R}}{3}\right)\triangle y \end{bmatrix}$$

$$\times \begin{bmatrix} k_{11}^{-1} \\ k_{12}^{-1} \\ k_{22}^{-1} \end{bmatrix} = \begin{bmatrix} P_{1L}-P \\ P-P_{1R} \\ P_{2L}-P \\ P-P_{2R} \end{bmatrix}. \qquad (10)$$

The upscaled permeability tensor can then be calculated with Eq. (8)

Experimental Results

Some results are shown here based on the above methodology and some 2D numerical experiments. We define κ to be a scalar field indexed by grid locations $(i,j)\in\tilde{\Omega}$. Then if κ is distributed according to a stationary GMRF with mean μ, it has density function given by

$$\pi(\kappa)\propto\exp\left\{-\frac{1}{2}(\kappa-\mu)^T W(\kappa-\mu)\right\},$$

where the fixed precision matrix W is required to be positive-definite and symmetric. The conditional distribution of any component κ_{ij} given all the remaining components $\kappa_{-\{ij\}}=\{\kappa_{kl},(k,l)\neq(i,j)\}$ is univariate normal with

$$\begin{aligned} E(\kappa_{ij}|\kappa_{-\{ij\}}) &= \mu+\sum_{(k,l)\neq(i,j)} w_{kl,ij}(\kappa_{kl}-\mu)/w_{ij,ij}, \\ V(\kappa_{ij}|\kappa_{-\{ij\}}) &= 1/w_{ij,ij}. \end{aligned} \qquad (11)$$

The precision matrix W is typically very sparse and parameterized by a small vector β. For the GMRF models considered here we use a third order neighborhood system and define

$$w_{ij,kl}=\begin{cases} 1 & \text{if } (i-k,j-l)=(0,0) \\ -\beta_0 & \text{if } (i-k,j-l)=(0,\pm1) \\ -\beta_1 & \text{if } (i-k,j-l)=(\pm1,0) \\ -\beta_2 & \text{if } (i-k,j-l)=(\pm1,\mp1) \\ -\beta_3 & \text{if } (i-k,j-l)=(\pm1,\pm1) \\ -\beta_4 & \text{if } (i-k,j-l)=(0,\pm2) \\ -\beta_5 & \text{if } (i-k,j-l)=(\pm2,0) \end{cases}$$

Thus the sum in (11) depends only on the 12 neighboring sites of (i,j). In general, it is required that any choice of β yields a symmetric, positive definite precision matrix W.

Diagonal Tensor Case In this case, each diagonal entry of the permeability tensor can be treated independently. Therefore, we only present the upscaling results for a scalar permeability field. Our first experiment is on a 2D rectangular domain. The physical dimensions of the medium are $100ft$ by $100ft$. We divide this domain into 256 cells in each coordinate direction and take this as a fine scale grid. To generate a diagonal permeability field on this fine grid, we specify a set of β parameters which encourage straw-like structures in the first coordinate direction and ensure that the first principal entry of the permeability tensor is parallel to the coordinate axis. We use Markov chain Monte Carlo method [23] to sample the GMRF *pdf*. The diagonal tensor field will be the GMRF sample κ times an identity matrix, i.e.,

$$\mathbf{k}_{ij} = \kappa_{ij} \begin{bmatrix} 1.0 & 0.0 \\ 0.0 & 1.0 \end{bmatrix} = \begin{bmatrix} k_{11} & 0.0 \\ 0.0 & k_{22} \end{bmatrix}_{ij}, \quad for \ \ (i,j) \in \tilde{\Omega}.$$

Fig. 3 shows a realization of the Gaussian MRF model with a set of parameters and its histogram.

For flow simulation on the fine grid, an boundary injector on the left of the physical domain is specified with a uniform constant pressure of $1000psi$ and a producer is assumed on the right boundary of the domain and specified with a constant pressure of $100psi$. The top and bottom boundaries are considered no flow. A constant porosity value of 0.27 and a negligible gravity effect are also assumed. The fluid viscosity is $1cp$. After solving the system of equations on the fine grid, we calculated the upscaled flow variables on the coarse scale grid using Eq.(5) and an upscaling factor $R = 2$. Hence, $\tilde{\Omega}^c = \{\Omega^c_{IJ}, I = 1, 2, ..., 128; J = 1, 2, ..., 128\}$. It should be pointed out that the upscaled side velocities satisfy the divergence free condition exactly.

The upscaled flow variable values are then used to calculate the diagonal permeability field on the coarser grid in terms of Eq.(4). It should be noted that to calculate k^c_{11} entry on the coarse grid, we only need the side velocities and pressures in the x-coordinate direction. In other words, we can only conserve fine scale flow in the x-direction. However, due to the permeability heterogeneity on the fine scale grid, solution of the system equations Eq.(3) does produce a non-zero component of side velocities in the y-coordinate direction, although very small compared to the side velocities in the x-direction. Fig. 4 shows the upscaled field of k_{11} in Fig. 3(a).

It is interesting to note both from the histograms and from the color maps that the upscaled field looks like a smoothed version of the fine-scale field. In particular, the mean of the upscaled field is approximately similar to that of the fine field and the variance of the upscaled field is reduced. This is very typical based on our observation of many upscaling results. It suggests that the upscaling transformation which operates on a fine stationary Gaussian MRF model and conserves fine scale flow properties in the mean flow direction is linear because the Gaussianity remains unchanged only under linear transformation.

To verify this, we generated 50 realizations for k_{11} on the fine scale grid and we upscaled these realizations following exactly the same way. Then we calculated and compared the statistics (sample means and variances) based on these realizations. It turned out that the sample means of the fine scale realizations and the upscaled realizations are statistically the same ($499.78md$ and $499.65md$) and the sample variance of the upscaled realizations is slightly larger than $1/R$ times the fine scale variance(1569.4 and 894.3 respectively). We did a lot of experiments on different sets of the fine scale model parameters (β's) and upscaling factors (R) and we obtained basically similar results. As an example, we plotted in Fig. 6 a realization of the fine scale GMRF model with another set of parameters and its histogram as well as the corresponding upscaled ones.

The above results support the following upscaling formula[22].

$$\mathbf{k}^c_{IJ} = \frac{1}{R^2} \sum_{i=1}^{R} \sum_{j=1}^{R} \mathbf{k}_{[(I-1)R+i][(J-1)R+j]} + \delta_{IJ} \qquad (12)$$

Where $\delta_{IJ} \sim \mathcal{N}(0, \varepsilon^2)$, independent of the fine field $\mathbf{k}$, is a zero mean, i.i.d normal variable with variance ε^2. This means that the upscaled permeability field is the arithmetic average of the fine grid field plus a zero mean i.i.d Gaussian field δ, the variance of δ is inversely proportional to the upscaling factor R.

An Example of Symmetric Tensor Case Mathematically speaking, Eq.(3) can be solved for a symmetric tensor permeability and cell center pressure as long as the coefficient matrix associated with side pressures and side velocities is invertible (four equations for four unknowns). There are some imposed assumptions and some physical constraints which may not be under control. Most importantly, the resulting permeability tensor on each coarse cell must be positive definite. In the example, we consider an areal problem with dimensions $200ft \times 200ft \times 1ft$, i.e., $\Omega = \{(x, y), x, y \in [0, 200]\}$. We divide this rectangular domain into 256 by 256 cells on the fine scale grid and use a GMRF model to generate a scalar permeability field κ. The prior mean and standard deviation for κ are $1000md$ and $31.6md$ respectively. A set of model parameters ($\beta_0 = 0.595, \beta_1 = -0.209, \beta_2 = 0.105, \beta_3 = 0.198, \beta_4 = -.179, \beta_5 = -.011$) were chosen to encourage wooden structures in the southwest to northeast direction.

The tensorial permeability field on this fine grid is obtained by

$$\mathbf{k}_{ij} = \kappa_{ij} \begin{bmatrix} 1.0 & 0.01 \\ 0.01 & 0.95 \end{bmatrix} \quad for \ \ (i,j) \in \tilde{\Omega}. \qquad (13)$$

Hence, k_{11}, k_{12} and k_{22} in each fine cell are totally correlated.

An injector is positioned at the lower left corner. It is in cell (1,1) on the fine grid and specified with a constant injection pressure of $1500psi$. A producer is at the upper right corner and is in the fine cell (256,256). It produces at a constant flowrate of $800B/D$. The outer boundaries are considered no flow. After solving Darcy's equation and the divergence free equation by our HMFE scheme, we upscaled the side velocities and side pressures by conserving fine scale fluxes and driving pressures. Using this information, we determined a symmetric tensorial permeability field on the upscaled grid assuming an upscaling factor of $R = 4$, i.e., 4×4 fine cells are upscaled into one coarse cell. Therefore, we have 64×64 cells on the upscaled grid and $\mathbf{k}^c = \{\mathbf{k}^c_{IJ}, I = 1, 2, ..., 64; J = 1, 2, ..., 64\}$.

It turned out that on some of the upscaled cells, the calculated permeability tensor is not positive definite. In other words, either $k_{11}^{-1} < 0$ or $k_{22}^{-1} < 0$ or $k_{11}^{-1}k_{22}^{-1} - k_{12}^{-1}k_{12}^{-1} < 0$. For example, on cell (31,31) of the upscaled grid, $k^c_{11} = -1469.2md$, $k^c_{22} = -1185.3md$, and $k^c_{12} = k^c_{21} = 2292.9md$. In particular, $k_{11}^{-1} > 0$, $k_{22}^{-1} > 0$, $k_{11}^{-1}k_{22}^{-1} - k_{12}^{-1}k_{12}^{-1} < 0$, which indicates that a physically meaningful permeability tensor based on the upscaled flow variable values within the HMFE method does not exist. Since the discrete divergence free equation is independent of cell scales by the conservation transformation of fine scale fluxes while the conservation of flow is a physically reasonable assumption, a possible explanation for these results would be that the HMFE discretization of Darcy's law on this upscaled grid cell is not valid if an upscaled symmetric, positive definite permeability tensor exists. Examination of the fine flow variables and the upscaled ones verifies this explanation. In Fig. 5, we show a typical case where the upscaled flow variables actually violate the HMFE discretization for Darcy's law.

Another case where the upscaled flow variables fail to produce useful HMFE formulation on an upscaled cell is that the coefficient matrix in Eq. (6) is such that the determinant of the inverse of the resulting permeability tensor is on the order of 0.001 or less, i.e., $k_{11}^{-1}k_{22}^{-1} - k_{12}^{-1}k_{12}^{-1} \approx 0$. In this case, the resulting solutions are far away from reasonable although the flow field can be honored exactly. For example, in the upscaled cell (26,11), $V_{1L} = 4.975 < V_{1R} = 5.229$, $V_{2L} = 4.138 > V_{2R} = 3.888$, but $P_{1L} = 1101.186 > P_{1R} = 1098.675$, $P_{2L} = 1100.931 > P_{2R} = 1098.952$. As a result, $k_{11}^{-1}k_{22}^{-1} - k_{12}^{-1}k_{12}^{-1} = 0.0013$ and $k_{11} = 10783.43md$, $k_{12} = -19382.80md$, $k_{22} = 39084.75md$.

The above two cases are very common in this back-solution upscaling process. Up to this point, we don't know how to correct this in a theoretically sound way. However, we would offer an alternative below when either of the cases of negative definiteness occurs. Further rigorous treatment is subject to ongoing research. We have noticed that the upscaled pressure always looks reasonable by any means, and it does not distinguish significantly from the volume averaged pressures as in the next example.

We have also recognized that the upscaling results are independent of the well conditions (or boundary conditions) due to incompressible flow where only pressure gradient matters. For example, turning the flowrate-specified producer into a pressure-specified one does not change the upscaling results. The actual well pressure values also have no effect on the upscaling results. For example, setting injector pressure to be $1.0psi$ and the producer pressure to be $0.0psi$ could not change the upscaled permeability values. Hence, the upscaled results are "intrinsic" to the fine permeability fields and incompressible single phase flow.

An Example of the Over-determined Symmetric Tensor Case Following the same procedure as in the symmetric permeability tensor case, we first generate a correlated permeability tensor field from the GMRF model, then solve the HMFE linear system of equations and upscale the flow variables by conserving fluxes and driving pressures. The coarse cell center pressure is determined by volume averaging fine cell pressures. Finally, we use singular value decomposition to compute a symmetric permeability tensor from a over-determined system in each upscaled cell.

Here, we present the results of the same physical problem and the GMRF model as in the unique symmetric tensor case for comparison. The only difference is that the tensor field on the fine grid is now calculated by

$$\mathbf{k}_{ij} = \kappa_{ij} \begin{bmatrix} 1.0 & -0.005 \\ -0.005 & 0.95 \end{bmatrix} \quad for\ (i,j) \in \tilde{\Omega}. \qquad (14)$$

meaning that a pressure drop in the x-direction could cause a negative flux in the y-direction on the fine scale grid.

Solutions of the pressure and divergence free equations on the fine scale grid were checked and then conservatively upscaled through Eq. (5). The upscaled permeability tensor results by singular value decomposition method were also carefully examined. The results still show the same problems as in the last example. We don't repeat any explanation here. Instead, we list some of the results on the diagonal of the physical domain in Table 1 as verifications. Notice that there are some negative k_{11}'s and k_{22}'s and the value of k_{11} in the upscaled cell (49,49) is $3145.06md$ which is too large. Notice also that k_{21} is basically on the same order of magnitude as k_{11} or k_{22} which is not reasonable compared to the fine scale tensors.

Discussion and A Feasible Alternative

The above upscaling results have given rise to some difficulties which make the simulation-based upscaling approaches quite questionable, specifically in tensorial permeability field cases. Most problematically, the HMFE

discretization of Darcy's law on upscaled cells may not be valid. As a result, an upscaled positive definite permeability tensor can not be determined from the conserved flow variables. However, the HMFE method is one of very few discretizations that allow conservative upscaling. With block-centered difference methods, it is unknown how to find a coarse permeability field so that the coarse equations produce flow consistent with the upscaled fine volume flux and pressure.

It is obvious with the HMFE method that in order to obtain a positive definite tensor on an upscaled cell, some conditions on the conserved upscaling fluxes and pressures must be satisfied from the solution viewpoint of a nonsingular linear system. These conditions can be derived from the system directly without any difficulty. For example, to have a positive definite permeability tensor from Eq. (6), the upscaled values of V_{1L}, V_{1R}, V_{2L}, V_{2R} and P_{1L}, P_{1R}, P_{2L}, P_{2R} must be such that the resulting $k_{11} > 0$, $k_{22} > 0$ and $k_{11}k_{22} - k_{21}k_{21} > 0$. However, conserving fine scale fluxes and pressures for V_{1L}, V_{1R}, V_{2L}, V_{2R} and P_{1L}, P_{1R}, P_{2L}, P_{2R} on a coarse cell has no guarantee of meeting these conditions, and thus the positive definiteness of the resulting tensor. Release of the symmetry assumption on the permeability tensor may partially resolve this problem, but we don't see reasons that this problem could be completely solved. We did not try this since the HFME method assumes symmetric permeability tensors.

Although Darcy's law is derivable from Navier-Stokes equation under the assumption of local homogeneity, this does not mean that Darcy's law is valid in heterogeneous fields going from fine scale to coarse scale with arbitrary boundary conditions. In the Appendix, we present step-by-step the upscaling formulas through the simplest possible case and demonstrated with two specific examples that there is no guarantee that a symmetric permeability tensor which satisfies the the HMFE formula, i.e., the discrete Darcy's law, on an upscaled cell and preserves positive definiteness at the same time, can be obtained.

Based on our experience, it is still feasible to determine an upscaled positive definite permeability tensor field from the HMFE scheme and the GMRF model, as was done by other researchers using finite difference schemes and Gaussian permeability models. But a two step procedure must be utilized. For example, one can create a synthetic flow field on a fine symmetric positive definite field by imposing a pressure gradient on physical boundaries first in the x-coordinate direction and closing the boundaries in the y-direction, then compute an upscaled field following the procedure in the second example (unique symmetric case), keep the results for entries k_{11} and k_{12} (these entries would look reasonable), but throw away the results of entry k_{22}. Subsequently and by the same token, one could obtain results by switching the boundary conditions in the x- and y-coordinate directions. This time, take only k_{12} and k_{22}. Normally, k_{12} from the first step should be different from the k_{12} of the second step, meaning the resulting permeability tensor is not symmetric. To force symmetry, a simple approximation would be the arithmetic average of the two. Let's designate this average by $\bar{k}_{12}$. Usually, the resulting k_{11}, $\bar{k}_{12}$ and k_{22} would give a positive definite tensor on each upscaled cell.

The problem with this process, however, is that the fine scale flow field can not be honored totally and there is no theoretical justification on how good the upscaling results would be, except that a full-field real simulation and a comparison with fine scale simulation results are made. As an illustration, we present some results obtained in such a way. In Fig. 7(a), we plotted a realization of the GMRF model, taken as k_{11} on the fine scale grid with 256×256 cells. The GMRF model parameters are $\beta_0 = 0.440, \beta_1 = 0.227, \beta_2 = -0.042, \beta_3 = -0.080, \beta_4 = -.051, \beta_5 = -.005$. The physical dimensions are $200ft$ by $100ft$. The boundary conditions used in the first step are constant pressures over the left/right boundaries and no-flow top/bottom boundaries. In Fig. 7(b), the upscaled k_{11} entry from the first step is plotted. Visually, most of the heterogeneity structures are preserved in the upscaled field, which makes physical sense. We have also plotted the histograms with statistics for both the fine scale field and the upscaled one. The permeability tensor on the fine scale grid was set similarly as in Eq. (14). In Fig. 8, we compared the histograms of the off-diagonal entry k_{12} on the fine grid and the upscaled grid from the first step. Their statistics are significantly different and some extreme values also appeared, which raise another caution in practical applications.

Conclusion

We have implemented a simulation-based upscaling procedure in our AMR code libraries for tensorial peameability fields in two dimensions based on the HMFE numerical scheme and a GMRF permeability model. We have tried three cases. In the first case, we assumed an upscaling coefficient R and a diagonal permeability tensor on both the fine scale grid and the upscaled grid. It turned out that for any of the realizations from the various GMRF models we considered, the upscaled permeability field is actually a "smoother" version of the fine scale field. This is consistent with both the averaging properties of the GMRF model and geological experience. In the second case, we assumed a nonzero off-diagonal tensor field but kept the symmetry of the tensor. We start from a positive definite tensor field on a geological fine grid, simulate a synthetic single phase, incompressible flow based on the HMFE discretization on the fine domain, then we back solve the discretized HMFE system in the same form for permeability tensors on an upscaled grid in terms of the conserved flow fluxes and driving pressures. There were two subclasses

depending on how the upscaled cell-center pressures are computed. We solve the linear system analytically if the pressures are solved simultaneously with the entries of the tensor inverse, while we apply the singular value decomposition for an over-determined system where the cell-center pressures are calculated independently by volume averaging the corresponding fine cell center pressures. We have demonstrated that a positive definite, physically meaningful permeability field on coarser scales can not always be determined. We think that these results are not specific to the HMFE method and the GMRF model, but are general to the simulation-based upscaling approaches based on other numerical schemes and other permeability models.

We have also tried a two step upscaling procedure done by many others for a positive definite tensor field on coarser grids. The upscaling results look reasonable, but with many large off-diagonal values. Moreover, these upscaling results don't conserve fine flow. In other words, if the upscaled tensor field obtained in this way were used to simulate on the upscaled grid, then it would not produce the same fluxes and pressures as those upscaled from the fine flow simulation. So we recommend that they are used with caution for real, full field simulation.

References

1. Trangenstein J. A., Bi, Z. and Ilya M. D.: "Multi-Scale Iterative Techniques and Adaptive Mesh Refinement for Flow in Porous Media," Invited by *Adv. in Water Resources*, 2001.
2. Renard, Ph. and Marsily G.: "Calculating Equivalent Permeability: a Review," *Adv. in Water Resources*, Vol. 20, Nos 5-6, p253-278, 1997.
3. Wen, X. H., Gomez-Hernandez, J. J.: "Upscaling Hydraulic Conductivities in Heterogeneous Media: An Overview," *Journal of Hydrology*, Vol. 183, ix-xxxii, 1996.
4. Wen, X. H., Durlofsky L. J., Lee S. L. and Edwards M. G.: "Full Tensor Upscaling of Geologically Complex Reservoir Descriptions," SPE 62928, 2000.
5. Sanchez-vila, X., Carrera, J., Girardi, J. P.: "Scale Effect in Transmissibility," *Journal of Hydrology*, Vol. 183, p1-12, 1996.
6. Tran, T.: "The Missing Scale and Direct Simulation of Block Effective Properties," *Journal of Hydrology*, Vol. 183, p37-56, 1996.
7. White, C. D., Horne, R. N.: "Computing Absolute Transmissibility in the Presence of Fine-Scale Heterogeneity," SPE 16011, 1987.
8. Indelman, P., Dagan, G.: "Upscaling of Permeability of Heterogeneous Formations. Part 1: General Approach and Application to Isotropic Media," SPE 22206, 1990.
9. Dagan, G.: "Models of Groundwater Flow in Statistically Homogeneous Porous Formations," *Water Resources Research*, Vol. 15, No. 1, p47-63, 1979.
10. Almeida, J. A., Soares, A., Pereira M. J. and Daltaban, T. S.: "Upscaling of Permeability: Implementation of a Conditional Approach to Improve the Performance in Flow Simulation," SPE 35490, 1996.
11. Lee, J., Kasap, E., Kellkar, M.: "Analytical Upscaling of Permeability for 3D Gridblocks," SPE 27875, 1996.
12. Ribeiro, R. F., Romen, R. K.: "Computing the Effective Permeability by Finite Differences, Finite Elements and Mixed-Hybrid Finite Elements," SPE 39068, 1997.
13. Durlofsky, L. J., Behrens, R. A., Jones, R. C., Bernath A.: "Scale Up of Heterogeneous Three Dimensional Reservoir Descriptions," SPE 30709, 1997.
14. Durlofsky, L. J.: "Numerical Calculation of Equivalent Grid Block Permeability Tensors for Heterogeneous Porous Medium," *Water Resources Research*, Vol. 27, p699-708, 1991.
15. Durlofsky, L. J., Milliken, W. J., Bernath A.: "Scale Up in the Near-Well Region," SPE 51940, 1999.
16. King P. R.: "The Use of Renormalization for Calculating Effective Permeability," *Transport in Porous Media*, Vol. 4, p37-58, 1989.
17. Pickup, E. G., Carruthers, D.: "Effective Flow Parameters for 3D Reservoir Simulation," SPE 35495, 1996.
18. Journel, A. G., Deutach, C. and Desbarats, A. J.: "Power Averaging for Block Effective Permeability," SPE 15128, 1986.
19. Besag J.: "Spatial Interaction and the Statistical Analysis of Lattice Systems (with discussion)," Journal of the Royal Statistical Society, Vol. 36, p192–236, 1974.
20. Tjelmeland H. and Besag J.: "Markov Random Fields with Higher-Order Interactions," Scandinavian Journal of Statistics, Vol. 25, p415-433, 1998.
21. Geman S. and Geman D.: "Stochastic Relaxation, Gibbs Distributions, and the Bayesian Restoration of Images," IEEE Transactions on Pattern Analysis and Machine Intelligence, Vol. 6, p721-741, 1984.
22. Chellappa R. and Jain A. K.(Editors): "Markov Random Fields : Theory and Application," Academic Press, 1993.
23. Besag J., Green P. J., Higdon D. and Mengersen M.: "Bayesian Computation and Stochastic Systems (with discussion)," Statistical Science, Vol. 10, p3-66, 1995.

Appendix A: Upscaling formulas and examples on a 2×2 fine grid: questioning Darcy's law from fine scale to coarse scale

We consider a 2D unit-square domain, $\Omega = \{(x, y), x, y \in [0.0, 1.0]\}$. For simplicity, we specify uniform pressures on the four boundaries, $P(0.0, y) = p_{x0}$, $P(1.0, y) = p_{x1}$, $P(x, 0.0) = p_{y0}$, $P(x, 1.0) = p_{y1}$. On the fine scale, we divide the domain into 2 by 2 cells with equal sizes, i.e., $\tilde{\Omega} = \cup_{i=1}^{2} \cup_{j=1}^{2} \Omega_{ij}$. Each cell has a piecewise constant permeability tensor, $\mathbf{k}_{ij}$, as shown below.

Given all the information, we can easily solve for the side pressures inside the domain, i.e., $P_{\frac{1}{2},1}$,$P_{\frac{1}{2},2}$, $P_{1,\frac{1}{2}}$, $P_{2,\frac{1}{2}}$, based on the boundary pressures and the continuity of fluxes in the x and y directions.

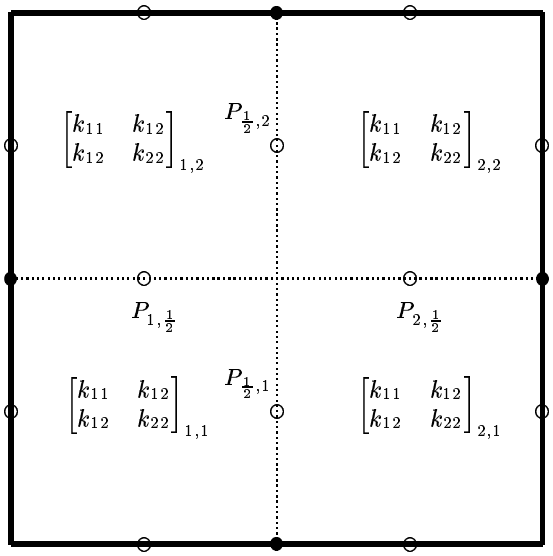

To show this process, we first write Eq. (3) in each fine cell as

$$\begin{bmatrix} V_{1L}\triangle y \\ V_{1R}\triangle y \\ V_{2L}\triangle x \\ V_{2R}\triangle x \\ P \end{bmatrix} = \begin{bmatrix} M1 & M2 & M4 & M7 & m1 \\ M2 & M3 & M5 & M8 & m2 \\ M4 & M5 & M6 & M9 & m3 \\ M7 & M8 & M9 & M10 & m4 \\ m1 & m2 & m3 & m4 & b \end{bmatrix}_{ij} \begin{bmatrix} P_{1L} \\ -P_{1R} \\ P_{2L} \\ -P_{2R} \\ -q \end{bmatrix}, \tag{B-1}$$

Where the symmetric matrix at the right hand side represents the inverse of the coefficient matrix in Eq. (3) and is related to the permeability tensor of each cell (i,j). For example,

$$M1 = \left[\frac{(4k_{11}^{-1}+k_{22}^{-1})k_{22}^{-1} - 3k_{12}^{-1}k_{12}^{-1}}{(k_{11}^{-1}+k_{22}^{-1})(k_{11}^{-1}k_{22}^{-1}-k_{12}^{-1}k_{12}^{-1})}\right]_{i,j},$$

$$m1 = \left[\frac{1}{2}\frac{k_{22}^{-1}}{(k_{11}^{-1}+k_{22}^{-1})}\right]_{i,j}, \quad b = \left[\frac{1}{12}\frac{k_{11}^{-1}k_{22}^{-1}}{(k_{11}^{-1}+k_{22}^{-1})}\right]_{i,j}.$$

The side pressures, $P_{\frac{1}{2},1}$,$P_{\frac{1}{2},2}$, $P_{1,\frac{1}{2}}$ and $P_{2,\frac{1}{2}}$, are determined by a system of equations that couples the grid cells,

$$\begin{aligned}
P_{\frac{1}{2},1} &= [(M1)_{1,1} + (M3)_{1,1}]\, r_1 + (M8)_{1,1}\, r_3 + (M7)_{2,1}\, r_4, \\
P_{\frac{1}{2},2} &= [(M1)_{2,2} + (M3)_{1,2}]\, r_2 + (M5)_{1,2}\, r_3 + (M4)_{2,2}\, r_4, \\
P_{1,\frac{1}{2}} &= (M8)_{1,1}\, r_1 + (M5)_{1,2}\, r_2 + [(M6)_{1,2} + (M10)_{1,1}]\, r_3, \\
P_{2,\frac{1}{2}} &= (M7)_{2,1}\, r_1 + (M4)_{2,2}\, r_2 + [(M6)_{2,2} + (M10)_{2,1}]\, r_4.
\end{aligned}$$

Where

$$\begin{aligned}
r_1 &= (M2)_{1,1}\, p_{x0} + (M2)_{2,1}\, p_{x1} - [(M4)_{2,1} - (M5)_{1,1}]\, p_{y0}, \\
r_2 &= (M2)_{1,2}\, p_{x0} + (M2)_{2,2}\, p_{x1} + [(M7)_{2,2} - (M8)_{1,2}]\, p_{y1}, \\
r_3 &= [(M7)_{1,1} - (M4)_{1,2}]\, p_{x0} + (M9)_{1,1}\, p_{y0} + (M9)_{1,2}\, p_{y1}, \\
r_4 &= [(M5)_{2,2} - (M8)_{2,1}]\, p_{x1} + (M9)_{2,1}\, p_{y0} + (M9)_{2,2}\, p_{y1}.
\end{aligned}$$

which are associated with all the permeability tensors and the boundary pressures, p_{x0}, p_{x1}, p_{y0} and p_{y1}.

Knowing the side pressures and the piecewise constant permeability tensors, we can then compute the side velocities for each fine cell from Eq. (B-1) and the total flux on an upscaled coarse cell side. For example, the x-direction side fluxes of the first cell (1,1), $V_{-\frac{1}{2},1}\triangle y$ and $V_{\frac{1}{2},1}\triangle y$ can be calculated as,

$$\left[(M1)_{1,1}p_{x0} - (M2)_{1,1}P_{\frac{1}{2},1} + (M4)_{1,1}p_{y0} - (M7)_{1,1}P_{1,\frac{1}{2}}\right] \textit{ and}$$
$$\left[(M2)_{1,1}p_{x0} - (M3)_{1,1}P_{\frac{1}{2},1} + (M5)_{1,1}p_{y0} - (M8)_{1,1}P_{1,\frac{1}{2}}\right].$$

The total flux at the left boundary will be $\triangle y(V_{-\frac{1}{2},1} + V_{-\frac{1}{2},2})$. Total fluxes on any other upscaled cells can be computed in the same way.

With these side pressures, side velocities and fluxes, one can upscale the fine cells into 1×1, 1×2 or 2×1 coarse cells and analytically obtain the upscaled side pressures and velocities and subsequently the symmetric permeability tensors using Eq. (5) and Eq. (6) respectively.

As a numerical example, assume $p_{x0} = p_{y0} = 1.0$, $p_{x1} = p_{y1} = 0.0$ and,

$$\mathbf{k}_{1,1} = \begin{bmatrix} 2.0 & 0.1 \\ 0.1 & 1.0 \end{bmatrix}, \quad \mathbf{k}_{1,2} = \begin{bmatrix} 3.0 & -0.2 \\ -0.2 & 2.0 \end{bmatrix},$$

$$\mathbf{k}_{2,1} = \begin{bmatrix} 3.0 & 0.2 \\ 0.2 & 1.0 \end{bmatrix}, \quad \mathbf{k}_{2,2} = \begin{bmatrix} 4.5 & -0.05 \\ -0.05 & 2.5 \end{bmatrix}.$$

For these permeability tensors, we computed the values of $M1$ through $M10$ for each cell. The side pressures are $P_{\frac{1}{2},1} = 0.63$, $P_{\frac{1}{2},2} = 0.16$, $P_{1,\frac{1}{2}} = 0.77$ and $P_{2,\frac{1}{2}} = 0.10$. If the four fine cells are upscaled into 1×1 coarse cell, then the total fluxes on the four boundaries are $\triangle y(V_{-\frac{1}{2},1} + V_{-\frac{1}{2},2}) = 4.24$, $\triangle y(V_{\frac{3}{2},1} + V_{\frac{3}{2},2}) = 3.56$, $\triangle x(V_{1,-\frac{1}{2}} + V_{2,-\frac{1}{2}}) = 2.61$ and $\triangle x(V_{1,\frac{3}{2}} + V_{2,\frac{3}{2}}) = 3.28$, respectively. The conservative upscaled permeability tensor would be

$$\mathbf{k}^c_{1,1} = \begin{bmatrix} 0.48 & 3.42 \\ 0.1 & -0.47 \end{bmatrix},$$

which is apparently unreasonable. But if the four cells are upscaled into 2×1 cells, then the resulting permeability tensors would be

$$\mathbf{k}^c_{1,1} = \begin{bmatrix} 4.81 & 0.79 \\ 0.79 & 1.17 \end{bmatrix}, \textit{ and } \mathbf{k}^c_{2,1} = \begin{bmatrix} 5.17 & 1.31 \\ 1.31 & 0.77 \end{bmatrix},$$

which are actually positive definite.

It is clear enough from the above expressions and examples that the fine flow variables (side pressures and velocities) are all dependent on the permeability tensors in the entire domain and the pressures on all the four boundaries, so are the upscaled side pressures and side velocities. Consequently, there is no guarantee that a symmetric permeability tensor which satisfies exactly the HMFE equation (discrete Darcy's equation), i.e., Eq. (3), on the upscaled cell and preserves positive definiteness of the tensor at the same time, can be obtained.

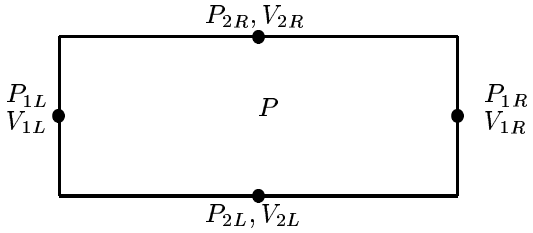

Figure 1: A rectangular element and its flow variables; P-cell pressure; P_{1L}, P_{1R}, V_{1L} and V_{1R} are side pressures and velocities in the x-direction; P_{2L}, P_{2R}, V_{2L} and V_{2R} are side pressures and velocities in the y-direction.

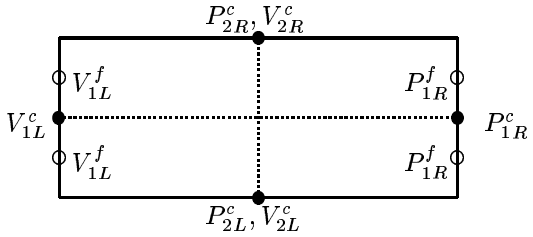

Figure 2: Upscaled flow variables by preserving fluxes and pressures from the fine grid. Here 2×2 fine cells are upscaled to one coarse cell (R=2).

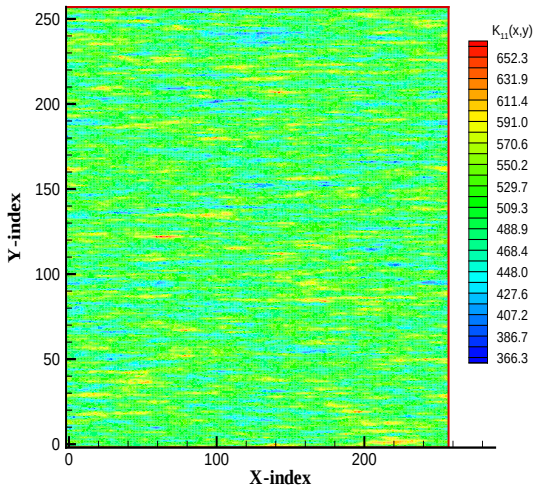

(a) A realization of $K_{11}(x, y)$.

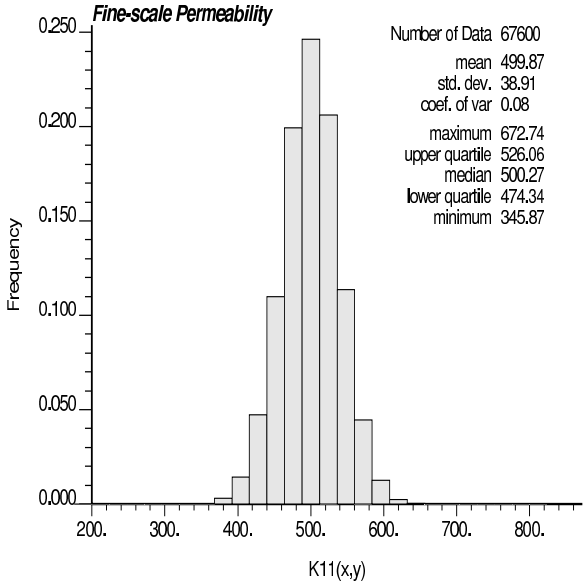

(b) The histogram of the realization.

Figure 3: (a) A realization of $K_{11} = \kappa$ generated from the permeability model on the fine-scale grid (256×256 cells), Model parameters are $\beta_0 = 0.499, \beta_1 = 0.001, \beta_2 = \beta_3 = \beta_4 = \beta_5 = 0.0$. The final permeability tensor field is set to be diagonal, so $k_{11} = k_{22}$; (b) The histogram of the realization.

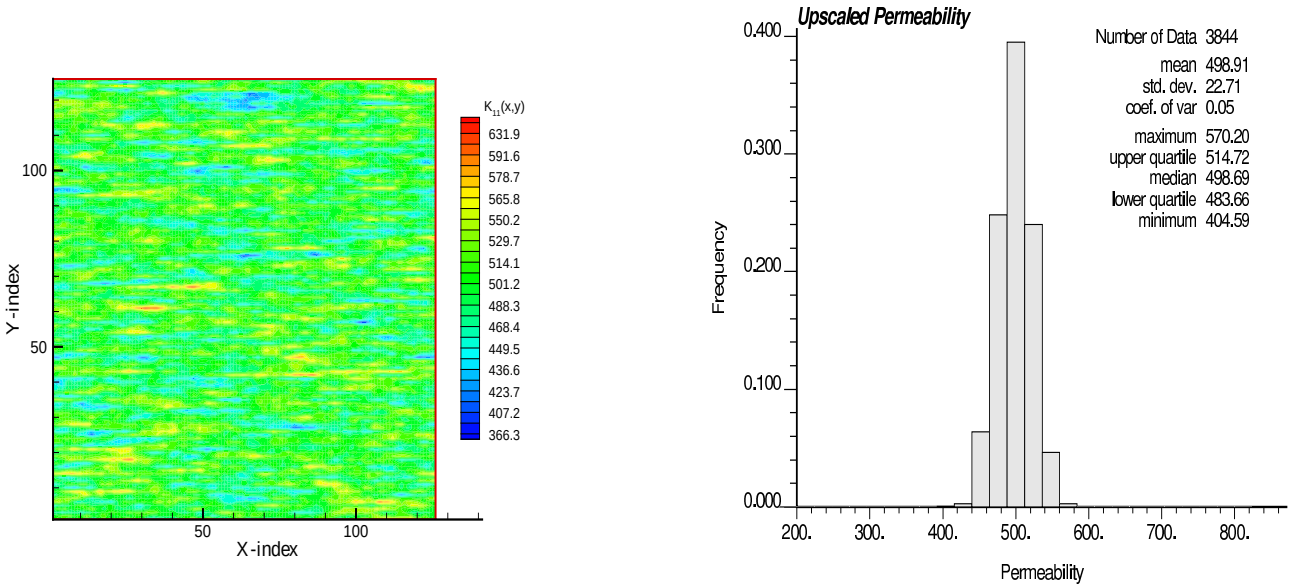

(a) The Upscaled field of $K_{11}(x, y)$

(b) The histogram of the upscaled field

Figure 4: The upscaled version of K_{11} in Fig. 3(a) and its histogram.

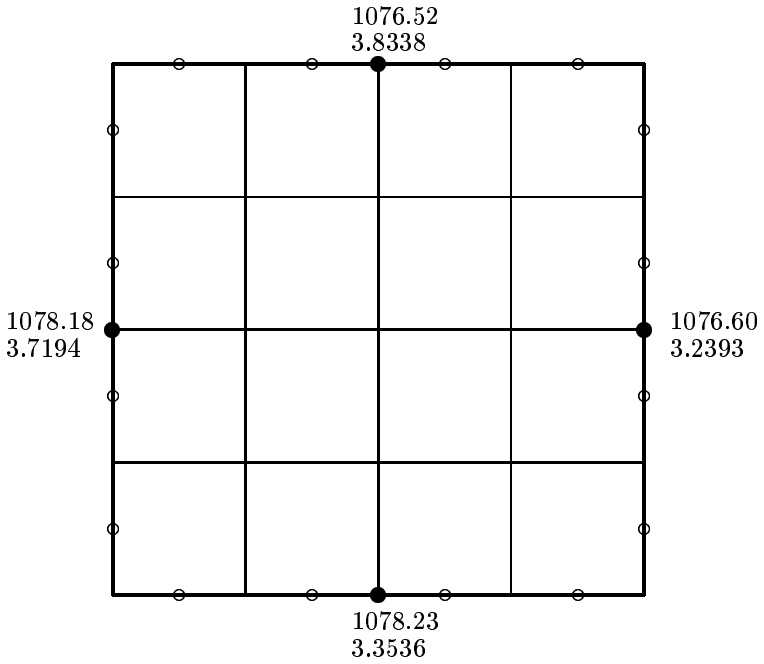

Figure 5: A coarse cell, its upscaled side pressures in *psi* (above) and velocities in ft/day (below). Blank circles represent the fine cell edges for pressure and velocity calculations. Here on the upscaled cell edges (dots), $P_{1L} = 1078.18 > P_{1R} = 1076.60$, $V_{1L} = 3.7194 > V_{1R} = 3.2393$, but $P_{2L} = 1078.23 > P_{2R} = 1076.52$ and $V_{2L} = 3.3536 < V_{2R} = 3.8338$, which are against the discretized Darcy's law.

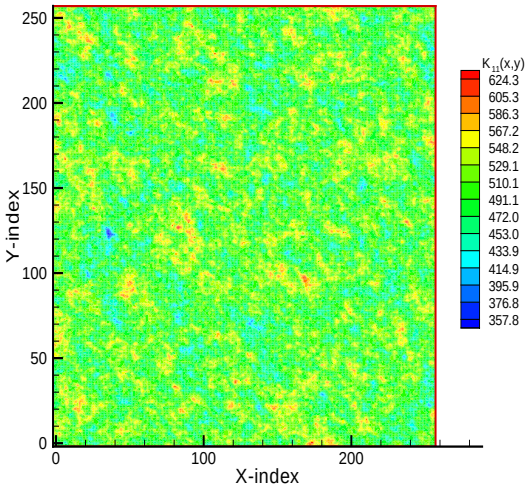

(a) Another realization of $K_{11}(x, y)$

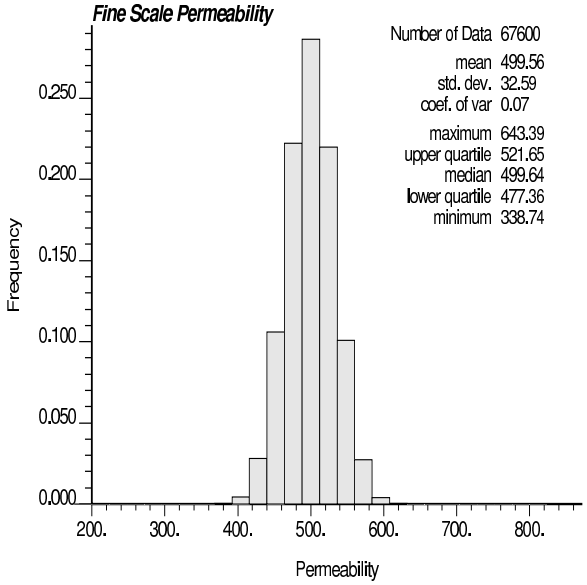

(b) The histogram of the realization in (a)

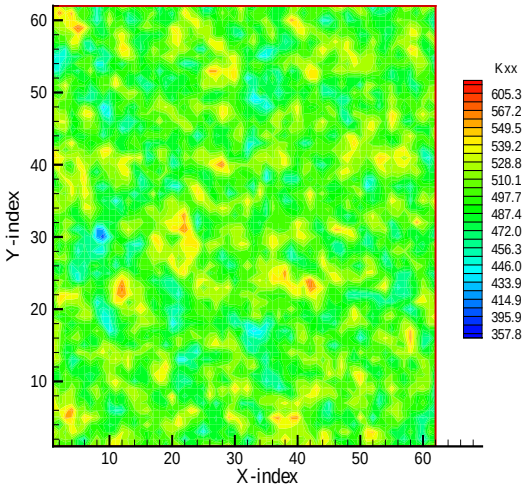

(c) The upscaled field of $K_{11}(x, y)$

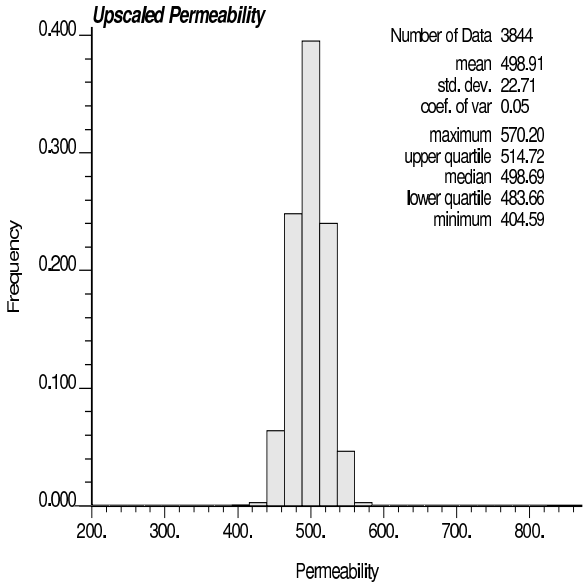

(d) The histogram of the realization in (c)

Figure 6: (a) A realization of K_{11} generated from the permeability model on the fine-scale grid (256×256 cells), Model parameters are $\beta_0 = 0.440, \beta_1 = 0.227, \beta_2 = -0.042, \beta_3 = -0.080, \beta_4 = -0.051, \beta_5 = 0.005$. The final permeability tensor field is set to be diagonal and $k_{11} = k_{22}$; (b) The histogram of the realization (a); (c) The upscaled field of (a); (d) The histogram of field (c).

Cell Index		Upscaled Permeability Tensor(md)		
I	J	k_{11}	$k_{12} = k_{21}$	k_{22}
10	10	0.30287232E+03	0.62393668E+03	0.29237356E+03
11	11	0.34384168E+03	0.70907771E+03	0.31788879E+03
12	12	0.18205100E+03	0.76811796E+03	0.22095725E+03
13	13	0.49225238E+03	0.42729257E+03	0.51334842E+03
14	14	0.22400155E+03	0.75697603E+03	0.27599606E+03
15	15	0.84850335E+03	0.13511769E+03	0.78111848E+03
16	16	0.70049641E+03	0.29167871E+03	0.65414188E+03
17	17	0.33120042E+03	0.58044404E+03	0.41806250E+03
18	18	-0.27919004E+03	0.12035826E+04	-0.21924916E+03
19	19	0.14328685E+03	0.74190652E+03	0.26156108E+03
20	20	0.35328581E+03	0.58074057E+03	0.41341273E+03
21	21	-0.79656548E+02	0.95598855E+03	0.11097732E+03
22	22	-0.66190526E+02	0.10156474E+04	0.57826239E+02
23	23	0.27767379E+03	0.78481329E+03	0.22316908E+03
24	24	0.23816896E+03	0.69236757E+03	0.29796884E+03
25	25	0.11258960E+04	-0.17745953E+03	0.10279125E+04
26	26	0.58514379E+02	0.84570403E+03	0.15164194E+03
27	27	0.13955669E+04	-0.34390877E+03	0.12410409E+04
28	28	0.30838641E+03	0.50768581E+03	0.42338731E+03
29	29	0.30469579E+03	0.52210457E+03	0.44087930E+03
30	30	0.43833127E+03	0.48682382E+03	0.52443920E+03
31	31	-0.14133267E+04	0.22299714E+04	-0.11440370E+04
32	32	-0.18320740E+04	0.26523123E+04	-0.14918793E+04
33	33	-0.65275321E+04	0.70369162E+04	-0.55425692E+04
34	34	0.26624984E+03	0.73245079E+03	0.24072804E+03
35	35	-0.35966009E+02	0.10795870E+04	-0.47015243E+02
36	36	0.53675255E+03	0.43275022E+03	0.59827965E+03
37	37	0.31963194E+03	0.58339130E+03	0.38502030E+03
38	38	0.23793860E+03	0.66672595E+03	0.30154988E+03
39	39	0.92504759E+03	0.39705006E+02	0.88986937E+03
40	40	0.10718348E+04	0.10935371E+02	0.99514074E+03
41	41	0.75718540E+03	0.28802621E+03	0.71457392E+03
42	42	0.27278403E+03	0.70854383E+03	0.25377028E+03
43	43	-0.44288889E+03	0.12521720E+04	-0.17375048E+03
44	44	0.59453805E+02	0.99375697E+03	0.12365714E+03
45	45	0.20915352E+03	0.86697940E+03	0.18201474E+03
46	46	0.10324708E+04	-0.36529199E+01	0.97930119E+03
47	47	0.52848762E+03	0.47606503E+03	0.48980915E+03
48	48	-0.43059130E+03	0.12850088E+04	-0.26399429E+03
49	49	0.31450632E+04	-0.19502103E+04	0.27425746E+04
50	50	-0.55881188E+04	0.61670521E+04	-0.47901714E+04

Table 1: Upscaled permeability tensors for the overdetermined case

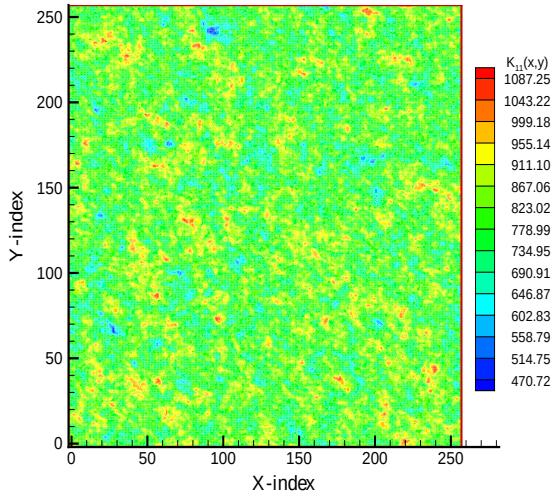

(a) k_{11} on the fine grid

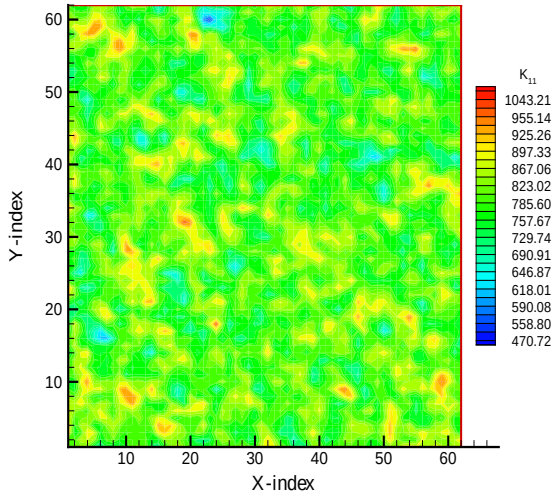

(b) k_{11}^c on the upscaled grid

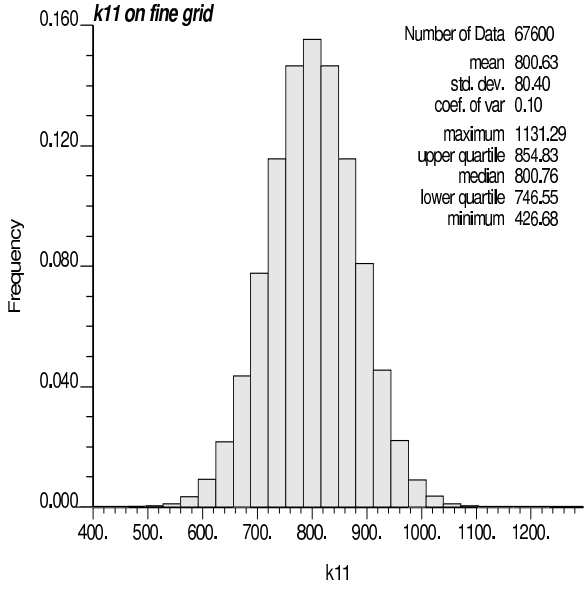

(c) The histogram of k_{11} in (a)

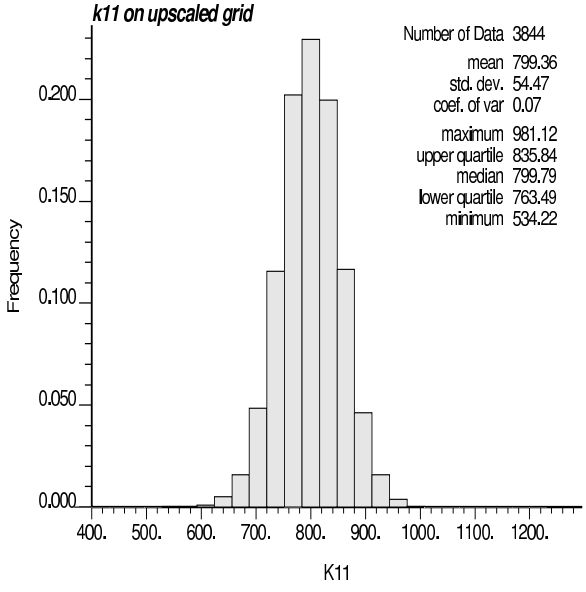

(d) The histogram of k_{11}^c

Figure 7: k_{11} entry from the two-step upscaling procedure: (a) The fine scale k_{11} field; (b) The upscaled field, k_{11}^c; (c) The histogram of fine scale field, k_{11}; (d) The histogram of k_{11}^c field.

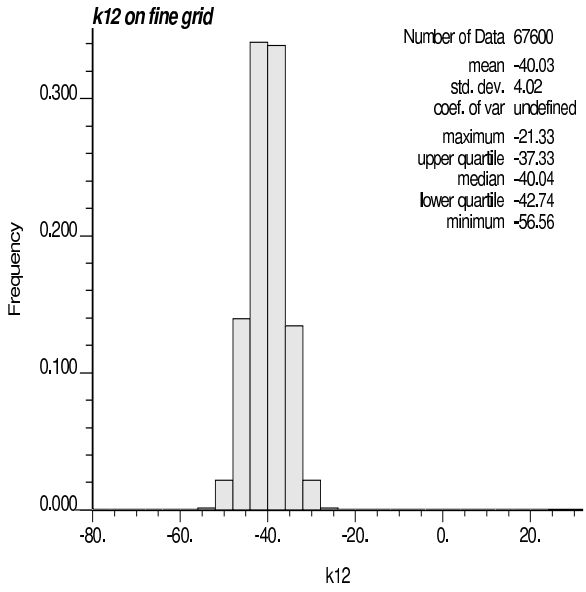

(a) The histogram of k_{12} on the fine grid

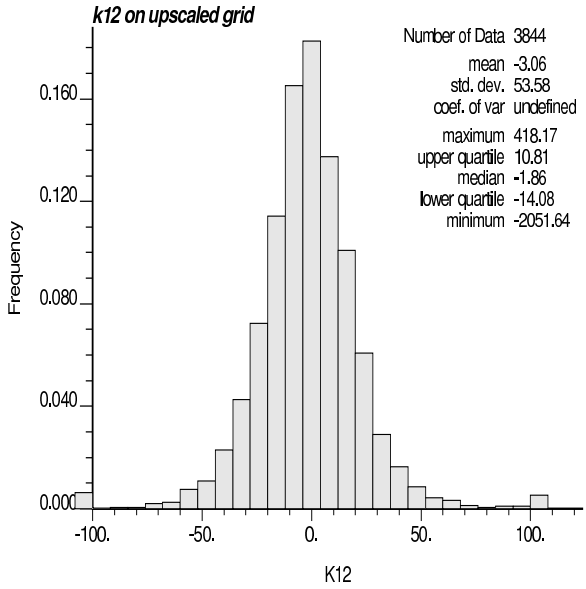

(b) The histogram of k_{12}^c on the upscaled grid

Figure 8: Comparison of the off-diagonal entry on the fine grid, k_{12}, and the upscaled grid, k_{12}^c. (a) The histogram of the fine scale k_{12} field; (b) The histogram of k_{12}^c field.